Journal of Nuclear Materials 396 (2010) 264–271

Contents lists available at ScienceDirect

Journal of Nuclear Materials

journal homepage: www.elsevier.com/locate/jnucmat

Nano-scale quasi-melting of alkali-borosilicate glasses under electron irradiation

Günter Möbus *, Michael Ojovan, Stuart Cook, Jim Tsai, Guang Yang

Dept. Engineering Materials, University of Sheffield, Mappin Street, Sheffield S1 3JD, UK

ARTICLE INFO

Article history:
Received 22 July 2009
Accepted 22 November 2009

ABSTRACT

Quasi-melting of micro- and nano-samples during transmission electron microscope irradiation of glassy materials is analysed. Overheating and true melting by the electron beam is shown not to be an explanation due to the ultra-sharp boundary between transformed and intact material. We propose that the observed fluidisation (quasi-melting) of glasses can be caused by effective bond breaking processes induced by the energetic electrons in the electron beam. The bond breaking processes modify the effective viscosity of glasses to a low activation energy regime. The higher the electron flux density the lower is the viscosity. Quasi-melting of glasses at high enough electron flux densities can result in shape modification of nano-sized particles including formation of perfect beads due to surface tension. Accompanying effects, such as bubble formation and foil bending are revisited in the light of the new interpretation.

© 2009 Elsevier B.V. All rights reserved.

1. Introduction

Irradiation behaviour of materials is a topic of high current interest. Two groups of research fields with major relevance of irradiation modification effects of materials, especially for ceramic and glassy materials, can be identified:

(i) Nuclear applications are an obvious example of permanent irradiation exposure, such as for construction materials or functional materials in current or future generation of nuclear reactors of fission and fusion type. Furthermore, vitreous materials have been chosen for several decades as the preferred option to immobilise nuclear waste and usage is planned to be expanded in forthcoming years. Special oxide-ceramics on the other hand are prospective host matrices for specific nuclear waste streams, less suitable for glasses, e.g. Pu.
(ii) Nanotechnology and its rapidly increasing number of proposed novel device architectures has generated a need to develop a large variety of nano-patterning techniques for surface modification, e.g. for substrate pre-patterning preceding growth processes, for direct data storage, or for nano-scale template replication processes.

The effect of irradiation on properties of ceramic and glasses has been examined extensively in the past (see [1–5]).

We can classify primary irradiation effects in glassy materials into *amorphisation, densification*, and *viscosity diminution* to be detailed in the following, while other observations of radiation-induced effects such as variations in refractive index, and mechanical properties have been identified as well [4,5].

Amorphisation of crystalline materials is the most evident result of irradiation and currently is intensely investigated for many potential nuclear waste host materials [4,6]. The amorphisation occurs at very high accumulated doses, e.g. critical amorphisation doses expressed in displacements per atom (dpa) are 0.2–0.3 for zirconolite, 0.3–0.4 for zircon, and far higher (>10) for zirconia and monazite.

Densification has been found, e.g. in fused silica on prolonged exposure to high-energy neutron, electron, and γ-ray radiation [7]. The densification of fused silica occurs also on exposure to photonic, e.g. laser radiation [8]. Both high-energy particle and laser radiation-induced densifications involve weakening of interatomic bonds and subsequent relaxation effects. The amorphous SiO_2 densification is caused by radiation-induced breaking of bonds and subsequent rearrangements of the SiO_2 ring network into more compact rings with the density eventually saturated with fluence [7]. Ion irradiation of amorphous solids also revealed stress relaxation and surface smoothing.

Viscous flow below melting temperature has been demonstrated [9–12]. The radiation-induced viscosity of amorphous silicon was estimated as 10^{13} Pa s, which was approximately four orders-of-magnitude smaller than thermally-activated shear viscosity of non-irradiated amorphous silicon at room temperature. The viscosity diminution in the presence of the ion beam was explained as due to the creation of broken bonds by the ion beam that otherwise would have to be created by thermal activation [9]. In situ wafer bending measurements demonstrated that radiation-enhanced viscous flow is Newtonian, i.e., the strain rate is

* Corresponding author.
E-mail address: g.moebus@sheffield.ac.uk (G. Möbus).

0022-3115/$ - see front matter © 2009 Elsevier B.V. All rights reserved.
doi:10.1016/j.jnucmat.2009.11.020

proportional to the stress [11]. It was also found that the radiation-enhanced fluidity increases with increasing radiation energy loss (or ion mass) and the radiation-induced viscosity is approximately inversely proportional to the nuclear energy loss [10]. This conforms well to viscous flow mediated by flow defects in which the viscosity is inversely proportional to the concentration of defects that contribute to viscous flow [13]. The averaged viscosity is inversely proportional to the number of flow defects created by radiation per unit length due to the fact that before any defects have annihilated, the number of flow defects per unit length is proportional to the radiation energy loss [9,10]. It is important to note evidences on changes in the activation energy of flow. It was found that for irradiated silicon the activation energy of viscosity was smaller than 0.3 eV compared to 1.8 eV of non-irradiated material. As the activation enthalpy for thermally activated flow in non-irradiated amorphous silicon is roughly equal to the energy required to break a bond (1.8 eV) this difference in activation energy demonstrated that the radiation-enhanced flow is not governed by bond breaking but rather by bond motion [9]. Studies of electron beam induced sintering of submicrometer particles demonstrated that the viscosity of amorphous silica drastically decreased by many orders-of-magnitude in a 200 kV TEM electron beam of 10 A/cm^2 current density on the specimen [15]. Although the temperature in those experiments was not higher than a few hundreds centigrade, the viscosity was as low as 10^8–10^9 Pa s, which would correspond to temperatures above 1400 °C. Such low viscosity of irradiated amorphous silica was attributed to the increase of defect concentration associated with the local structure [14]. While bond breaking is an appropriate picture for covalent materials, in ionic ceramics bonds are merely forces between ionic pairs at given distance. Irradiation acts here to alter coordination and bond distances, to alter the valence of adjacent cation or anion, or to generate point defects. Molecular dynamics simulations have also demonstrated that point defects (Frenkel pairs) provide an efficient mechanism for radiation-induced viscous flow of solids [15]. By simulation of the injection of interstitial and vacancy like defects it has been demonstrated that point defects induce the same amount of flow as the recoil events, indicating that point-defect-like entities mediate the flow process in solids even at 10 K. It was concluded that the radiation-induced flow does not require thermal spikes (local melting) and that point defects equally, or, in many cases, more efficiently provide the viscous flow, which earlier has been associated with thermal spikes (local melting) [15].

Electron beam irradiation damage in glasses is a topic of interest in concern with its consequences during the electron microscope studies and as an instrument to simulate the beta-decay irradiation damage [1–3]. Two main types of electron irradiation damage are radiolysis and knock-on damage [16]. Radiolysis involves damage to the electronic structure, including the breaking of the chemical bonds, which can lead to atom displacement as a secondary effect. Knock-on damage on the other hand involves the direct displacement of atoms via kinetic energy transfer, which could be followed by electronic structure rearrangement. In both cases point defects will be generated to various extents. A part of the electron beam energy is transferred to the specimen via electron–phonon scattering which causes specimen heating [17,18]. The higher the electron dose, the higher the energy transferred to the specimen. The amount of heating in the TEM is still a matter of controversy and debate. Estimates range from almost negligible temperature rise to true melting and sublimation. It was proposed that the quality of heat flow connection to the specimen support can affect the temperature change from a few degrees up to melting [16,19]. Ultra-fine hole drilling with nanobeams has been interpreted as achieving very localised melting and ablation by evaporation even in metals on well conductive supports due to kinetic heat transport delays [19]. There is more widespread agreement that heating can be significant for non-metals although estimates again largely vary on conditions. Si nanocrystals have been calculated to heat up by 20 °C [20], while SnO_2 nanorods heat up by 350 °C [21] Heating effects are typically managed using thinner specimens, coatings with conducting materials such as carbon or gold, or usage of cooling holders. Radiolysis is the main source of damage for glasses in 100–200 kV TEM and is caused by bond rupture and bond reconstruction with possible molecular oxygen formation; at high electron irradiation dose alkaline earth boroaluminosilicate glasses undergo phase separation into silicon rich and cation rich phases which is attributed to the rupture of silicon–oxygen–metal bonds [22–24].

This paper aims to give experimental and theoretical evidences on electron beam radiation-induced fluidisation (quasi-melting) of borosilicate glasses, based on our recent discovery of in situ (live) observation of the formation of glass beads out of any irregularly shaped micro- and nanofragment of this kind of glasses [25].

2. Experimental

The glasses studied in this work have been melted as described before [25,27], to result in compositions of Table 1, where "glass A" is a Ca-alumino-borosilicate, and "glass B" is a Li–Na Borosilicate (with Ce–Zr–Cr-doping).

Glasses were batched from reagent grade powders of oxides and carbonates, melted at 1400 °C for 5 h including stirring. Subsequently the melt was annealed for 1 h at 570 °C with cooling into metal forms with rectangular block shape.

Glass blocks of 300 g have been cut into slices from the inner material, and subsequently fractured and grinded by pestle-and-mortar into finest powders. After suspension of the powder in acetone to allow settling of the bigger particles, drops of the suspension have been dispersed on a Cu-grid with carbon film (Agar Scientific, Inc.). Amongst the variously shaped electron transparent fine micropowders, some fibre shaped fragments of 1–5 μm diameter have been found particularly useful for this study.

In a first experiment (Figs. 1 and 2), electron irradiation in a JEOL JEM-2010F field-emission gun TEM at 200 kV has been performed using the largest condenser aperture and spot size, giving a beam current of ~4 nA. Exposure of a sharp, rugged glass fibre end of glass A (Fig. 1a), fractured during preparation, has been performed for up to 30 min with a beam diameter of ~1000 nm (edge of beam visible in Fig. 1c). The transformation under these conditions is found to be very slow and can be easily observed in situ. In a first stage, for up to ~10 min, flattening of the rough surface is found as a primary process followed by a second stage comprising the slow overall shape transformation of the entire fragment until a seemingly perfect spherical bead shape is achieved. While the shape transformation at high magnification appears as a two-dimensional process, imaging with larger field-of-view in bright-field scattering contrast condition (Fig. 2) reveals a three-dimensional bead shape by means of thickness-contrast. Fig. 2 also proves that the transformation is exactly limited to a cylindrical region located inside the electron beam and sharply separated from the un-irradiated area, which seems to be completely unchanged. This observation is a first prove that pure thermal heating cannot

Table 1
Composition of glasses studied (mol.%).

Glass/oxide	SiO_2	B_2O_3	Al_2O_3	CaO	Li_2O	Na_2O	CeO_2	ZrO_2	Cr_2O_3
A	57	8	8	27	–	–	–	–	–
B	51.5	25.6	–	–	4.3	8.6	4.0	4.0	2.0

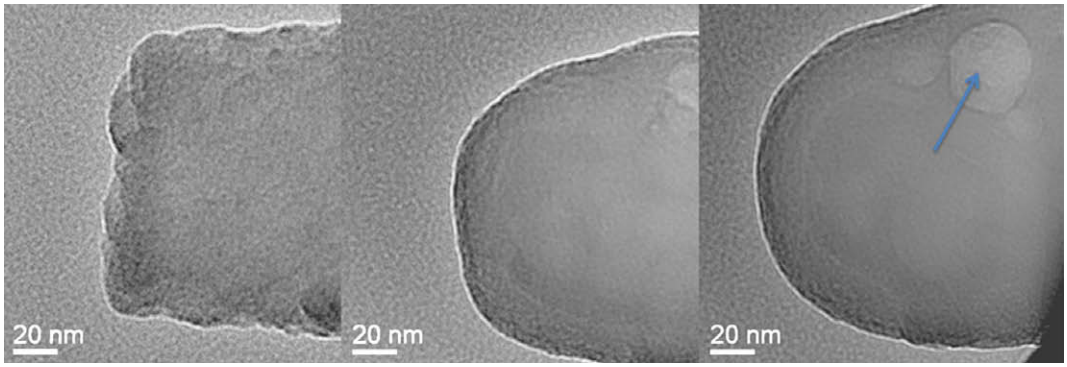

Fig. 1. Transformation of the rough end of a fractured Ca-alumina-borosilicate glass fibre (a) into a rounded fibre end (b) and finally a spherical glass bead (c) under electron irradiation in a moderately focused beam (~1000 nm diameter); JEM-2010F FEGTEM, total irradiation time 30 min. Arrows indicate the (transient) formation of bubble-type contrast.

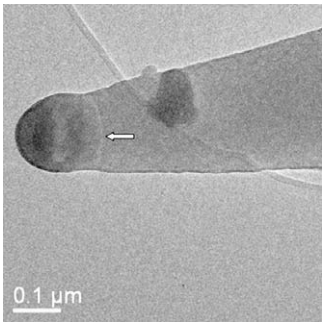

Fig. 2. Low-magnification image of the final result after the transformation of Fig. 1. In bright-field scattering contrast, the 3D bead shape can be estimated by the gray-levels, and the damage zone which was irradiated is clearly separated from the undamaged fibre by a white line (arrow). Fully defocused beam which does no longer sustain any further damage to the glass.

be the sole reason for this phenomenon, as temperature would not fall sharply at the edge of the beam. A secondary effect of interest, although not new as an observation (see [3] for the attribution of bubbles to molecular oxygen release), is the intermediate formation of bubble-type contrast in such glasses (see arrow in Fig. 1c). The bubbles seem to generate and subsequently grow during the second stage of shape transformation.

A second group of experiments has been carried out in a different TEM, a JEOL JEM 3010 LaB6 microscope, which allows to irradiate with even higher total emission current and higher voltage at 300 kV, however, due to the thermal emission filament this beam can be less focused than with our FEGTEM. We observe related phenomena which differ significantly in detail, this time using glass B, a Li–Na borosilicate, in its quenched state. In Fig. 3 glass fragments with more isotropic aspect ratio have been irradiated for several minutes during a "screening" routine while searching with a moderately focused beam for phase separation phenomena. A small percentage out of the thousands of particles of ~1000 nm diameter, have been found to spontaneously and unpredictably transform in less than a 10th of a second into perfect glass beads. Those particles which did not undergo the spontaneous transformation, could not be forced to do so using even longer and more focused irradiation. As all fragments on the carbon support film had identical composition, few criteria remain to explain the selectivity: size, shape and the detailed connectivity with the support film to transport heat. We note that the transformed particles are by one order of magnitude larger in radius than the radius of curvature of the rounded glass fibre of Fig. 1. In the same microscope the phenomenon of bubble generation has also been observed (Fig. 4), however, at a time scale when only the very initial steps of the above bead-transformation are taking place. Here, at a similar irradiation dose, however, applied via much higher current (focused beam) at much shorter exposure (3–10 s), widely dispersed bubbles form, initially of sub-10 nm size. Further exposure leads to growth and merger of bubbles before all bubbles disappear leaving a seemingly unchanged glass behind. glass B was used in the annealed state. This observation confirms earlier published results

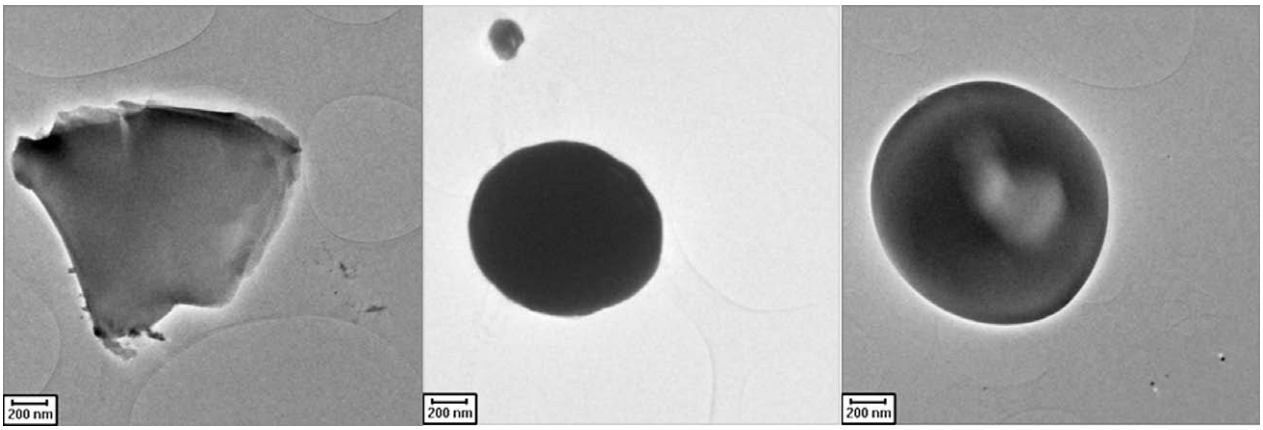

Fig. 3. Shape change of globular glass fragments into glass beads through electron irradiation via an explosive transformation of sub-second duration. A typical fragment (a) is compared to two (different) examples of transformed particles (b, c). JEM 3010 LaB6 TEM at 300 kV.

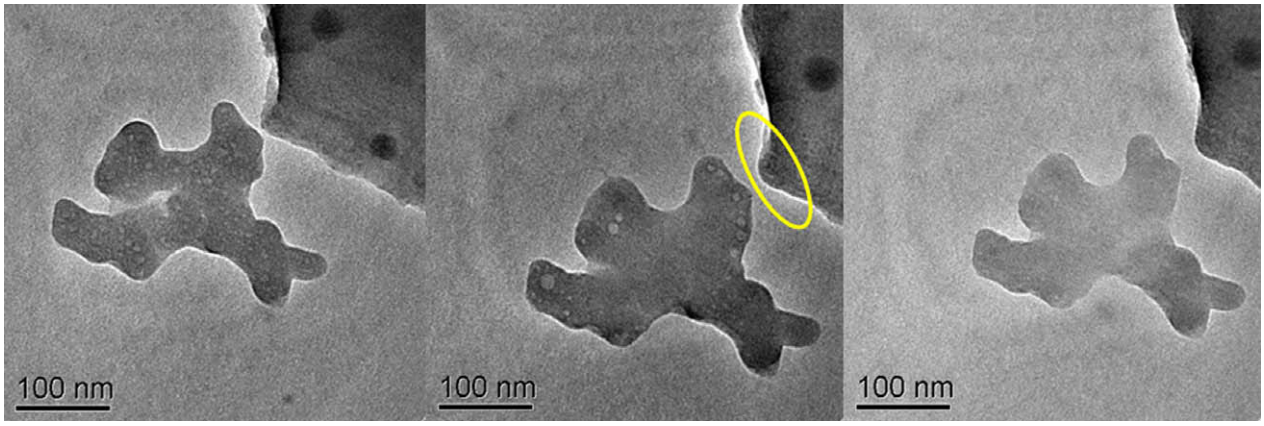

Fig. 4. Dynamical process of bubble formation (a), bubble growth and rounding of edges (encircled in yellow, b) and bubble annihilation. JEM 3010 LaB6 TEM at 300 kV.

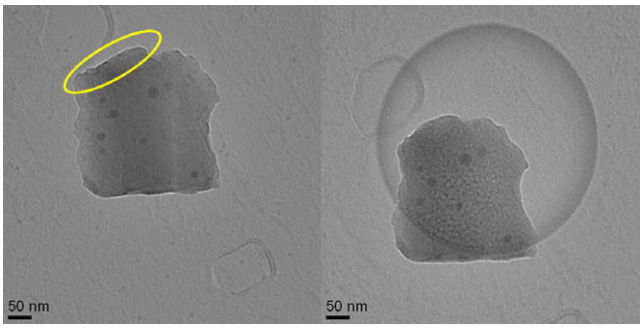

Fig. 5. Electron irradiation induced surface rounding (see region encircled at top left) in parallel to nanoscale phase separation of an alkali-borosilicate fragment on carbon support. JEM 3010, 300 kV. Electron beam exposed region is visible by circular carbon-deposited ring. The glass outside the beam is unaffected by both phenomena.

[3] about the link of bubbles to the removal of non-bridging oxygen. Detailed comparison of Fig. 4a and b show the rounding of a sharp edge (encircled in yellow[1]). Bubble formation is seen in our context as a parallel phenomenon which helps understanding the mechanism of shape transformation, as it is clearly impossible to be induced by temperature, but proves the kinetic activation role which the fast electrons play at a temperature far below melting point.

In a third experiment on the TEM JEM 3010, fluidity-induced surface roundening has been observed in parallel to nanoscale phase separation at exposure times which follow long after the transient bubble observation of Fig. 4 is finished. Fig. 5 shows a 300 nm diameter fragment of annealed glass B, which undergoes roundening in its top left corner (encircled in yellow), while at the same time all glass within the 600 nm diameter electron beam undergoes phase separation in two equally interconnected phases of structure size of 5–8 nm. Most probably we observed the spinodal phase separation in silica-rich and alkali-borate rich phases such as that which occur in "Vycor"-type glasses, a process that typically requires temperatures above 700 °C and times of the order of several hours [28]. Note that additionally visible Ce-oxide nanophases, formed during cooling and described in detail in [27] do not participate in this transformation. The picture is valuable as it clearly excludes temperature rise as the main reason for either effects of shape transformation or phase separation. Our reasoning is based on the unchanged bottom left corner which is outside the electron beam, visible by its deposited carbon imprint, but which would share a similar equilibrated temperature due to the long duration of the experiment.

While three-dimensional fragments seem to adopt a sphere as the low-viscosity morphology with lowest energy, a sample of annealed glass B in the shape of a free-standing thin film seems to have a tendency to roll-up (Fig. 6). Unlike all other samples in this work, the glass has been prepared by Argon ion milling/thinning which in its thinnest lamellae protruding into the central specimen hole can achieve extended thin areas of <10 nm thickness. The curvature induced into the thin film itself is probably a result of charging effects, as the glass thin film is not supported by any carbon film. This is also evident from the bright spikes at the top of the Fig. 6. The fact that the "brittle" material can sharply bend and roll with a bending radius of <100 nm, however, is believed to be the same irradiation induced fluidity enhancement identified to cause the bead formation of Figs. 1–3.

It has to be noted that literature also provides a catalytic explanation for transformation of particles into spherical balls: especially metal particles can induce a reaction with the carbon support film leading to formation of graphitic shells (onions) which encapsulate the particle during TEM observation [26]. Carbon contamination is another possible source of carbon ball formation. In our case, we do not observe any core–shell structure contrast and the estimated transformed volume is smaller or equal to the original one, rather than a growth into a bigger object, which can exclude the mentioned carbon encapsulation. We also conclude that surface roundening and C deposition seem completely separate, although parallel, phenomena from Fig. 5.

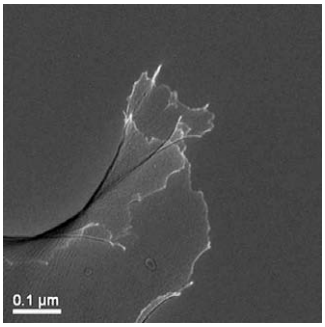

Fig. 6. Irradiation induced roll-up of initially flat ultrathin specimen of glass B, prepared by Ar ion milling.

[1] For interpretation of color in Figs. 4, 5 and 7–9, the reader is referred to the web version of this article.

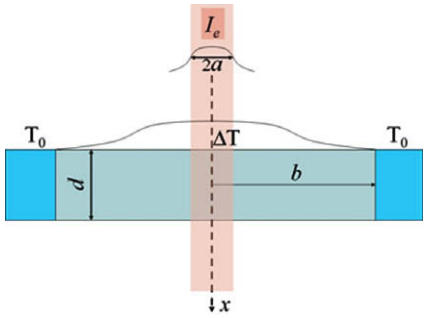

Fig. 7. Schematic of film irradiation by the electron beam. I_e is the electron flux density, $2a$ is the electron beam diameter, d is the glass sample thickness, b is the glass sample radius, T_0 is the temperature of sample holder and ΔT is the maximum temperature rise.

2.1. Consideration of heating effects

The electron irradiation of samples could result in heating effects. It has been shown however that thermal effects are insignificant for enough thin samples typically studied in transmission electron microscopes [29–35]. The temperature rise caused by absorption of electron radiation can be assessed using several theoretical models [29–31]. Fisher's model [29] which considers the temperature rise in thin metallic foils under intense electron irradiation as a function of beam conditions, electron energy, and the physical properties of the foil, is the widely used model for actual calculations in oxide materials [32–35]. Fisher evaluated the steady-state temperature increase caused by an electron beam by assuming that the specimen is of constant thickness, d. He assumed that the specimen is bound to a circular conductor of infinite conductivity held at a fixed temperature, T_0, with the electron irradiation incident to the center of the sample (Fig. 7), and that the radiative heat losses are negligible.

By assuming that the beam profile has a Gaussian distribution proportional to $\exp(-r^2/a^2)$, where r is the radial coordinate and a is the width of the Gaussian beam profile, Fisher's calculation yields for the maximum temperature rise ΔT which occurs in the center of the sample

$$\Delta T = I(\Delta E/d)(\gamma + 2\ln(b/a))/4\pi\kappa e \quad (1)$$

In this equation I is the beam current, ΔE is the energy loss per electron in a sample having a thickness d, γ is Euler's constant which equals 0.5772, b is the sample radius, κ is the thermal conductivity of the sample, and e is the electron charge. Eq. (1) shows that for constant ΔE the thinner the film the higher the temperature rise. It also demonstrates that a more focused beam with a higher b to a ratio causes a higher temperature rise. Let's assume that the total energy loss in the sample ΔE is negligible compared to the initial energy of electrons, $\Delta E \ll E$, which results in the requirement for sample thicknesses $d \ll E/(-dE/dx)$. In this case the term $\Delta E/d$ is approximately equal to $-dE/dx$, which is the stopping power for electrons in the sample. The stopping power of electrons can be calculated using the Bethe–Bloch equation [29–35]:

$$\begin{aligned} -dE/dx = {} & (Z\rho e^2/8\pi m v^2 \varepsilon_0^2)\left[\ln[E(E+mc^2)^2\beta^2/2I_{ex}^2 mc^2]\right] \\ & + (Z\rho e^2/8\pi m v^2 \varepsilon_0^2)\left[(1-\beta^2) - (2-\sqrt{1-\beta^2}-1+\beta^2)\ln 2\right. \\ & \left. +(1-\sqrt{1-\beta^2})/8\right] \end{aligned} \quad (2)$$

where Z is the atomic number of the sample target element, ρ its atomic density (from which the electronic density is derived as $n = N_A Z\rho/A$, where N_A is the Avogadro number and A is the atomic mass), ε_0 the dielectric constant, $\beta = v/c$, where v is the electron velocity and c is the speed of light, E is the electron energy, and I_{ex} is the average excitation energy for electrons in the target, which according to the Bloch approximation is taken as $I_{ex} \approx 10Z$ eV. Calculations using the Bethe–Bloch equation show that for electron energies E of the order of 200–400 keV the stopping power in silicate systems is of the order of 0.5–1 eV/nm consistent with [31–35]. This also means that samples should be thinner than several μm. For thin enough glass samples the maximum temperature rise can be assessed from (1). Eq. (1) gives a limit of $\Delta T \leqslant 2.4$ K for a beam current $\leqslant$10 nA, a beam radius of 500 nm (e.g. a electron beam current density $\sim$1 A/cm^2), a sample radius of 1000 nm, and a heat conductivity of 0.65 W/mK, which is typical for silicate glasses. The temperature increase is directly proportional to the electron beam current. The temperature rises are significant if the electron beam currents are of the order of $\sim$mA whereas nA currents result in negligible heat effects (see Fig. 8A). If the temperature of the sample holder is 300 K then the relative increase of temperature is $\Delta T/T_0 < 1\%$, then the increase of temperature is negligible for samples such as those used in our experiments. Larger diameter samples have a higher temperature rise, such that the more focused the electron beam the higher the temperature rise however the increase of temperature is logarithmic and very slow with (b/a) ratio (Fig. 8B).

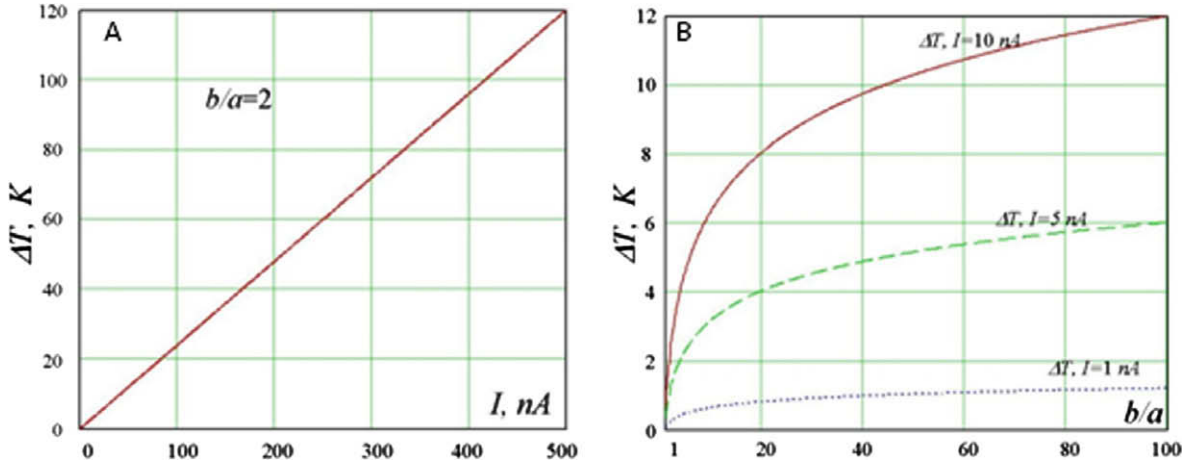

Fig. 8. Maximum temperature rise in the center of a thin electron beam irradiated silicate glass film as a function of electron beam current (A), and the maximum temperature rise as a function of sample radius to beam radius ratio for the electron beam currents I = 1, 5 and 10 nA (B).

Thus thermal effects are insignificant if glass samples are relative thin and the electron beam current is limited to nA range which is consistent with previous results [29–35]. We will consider first the qualitative effect of electron beam radiation on viscous flow in glasses and then will assess quantitatively the radiation-induced increase of fluidity.

3. Qualitative assessment of viscosity decrease

Viscous flow can be treated as due to flow defects in which the viscosity is inversely proportional to the concentration of defects that contribute to viscous flow [13]. The shear viscosity expressed in terms of the homogeneous density of broken bonds contributing to flow, C, can be written according to Mott as [13]:

$$\eta(T) = kT\exp(H/kT)/(4\pi r^3\gamma/3)^2 v_0 C, \tag{3}$$

where H is the activation enthalpy for flow, k is Boltzmann's constant, γ is the shear strain produced by the motion of a single defect, r is the radius of the defect, and v_0 is an attempt frequency of the defect to jump which is of the order of the Debye frequency.

The energetic electrons from the electron beam release their energy via exciting and ionising the matter. In the radiation field the flow defects, which are excitations of interatomic bonds in glasses, are created both by irradiation and thermal fluctuations such that

$$C = C_R + C_T, \tag{4}$$

where we assigned that the concentration of defects created by irradiation is C_R and those created by thermal fluctuations is C_T. The flow defects created by irradiation have a certain lifetime τ_b before any defects have annihilated. In the simplest model with one recombination channel when $C_R \ll C_0$, where C_0 is the total concentration of bonds, the kinetic of radiation-induced bond breaking is described by

$$dC_R/dt = k_b C_0 P_R - C_R/\tau_b, \tag{5}$$

where k_b is rate constant of bond breaking by radiation, P_R is the intensity of radiation (absorbed dose rate). In the steady state approximation $dC_R/dt = 0$ the concentration of radiation-induced broken bonds is

$$C_R = k_b\tau_b C_0 P_R, \tag{6}$$

and the concentration of broken bonds created by irradiation is directly proportional to the intensity of radiation P_R. An estimation of absorbed dose rate under electron beam irradiation (Gy/s) can be done using the equation [36,37] $P_R = 1.6\times10^{-13}(-dE/dx)I_e/\rho$, where $-dE/dx$ is the stopping power in MeV/cm, I_e is the electron flux density such as the electron microscope current, $e/s\ \mathrm{cm}^2$ and ρ is the density in $\mathrm{g/cm}^3$. For the absorbed dose rate (Gy/s) in the family of silicate glasses it was found that $P_R \cong 3\times10^{-11}I_e$ [37]. Hence the steady-state concentration of broken bonds created by irradiation in silicate glasses is

$$C_R = 1.6\times10^{-13}(-dE/dx)I_e k_b\tau_b C_0/\rho \tag{7}$$

Since both bond breaking rate constant (k_b) and lifetimes (τ_b) are unknown and difficult to calculate we will use for the concentration of electron beam broken bonds the expression:

$$C_R = f_{rad}C_0 = \alpha_e I_e C_0 \tag{8}$$

where $f_{rad} = 1.6\times10^{-13}(-dE/dx)I_e k_b\tau_b/\rho$ gives the relative concentration of radiation-induced broken bonds and the phenomenological constant α_e shows the efficiency of bond breaking and annihilation in the glass.

One can hence see from Mott's expression (3) that in an intensive radiation field when most of flow defects are formed by radiation, that is when $C_R \gg C_T$, the viscosity decreases proportionally to the intensity of irradiation (I_e):

$$\eta(T) = kT\exp(H/kT)/(4\pi r^3\gamma/3)^2 v_0\alpha_e I_e C_0 \tag{9}$$

Moreover it can be seen that the viscosity has in this case a low activation energy exactly equal to the enthalpy of flow (H). This result is confirmed by quantitative assessments given below.

4. Quantitative assessment of viscosity under electron beam radiation

To quantify the changes in the viscosity we will use data on viscosity of amorphous oxides [38–40] which show that the temperature dependence of viscosity is most exactly described by the two exponential equations:

$$\eta(T) = A_1 T[1 + A_2\exp(B/RT)][1 + C\exp(D/RT)], \tag{10}$$

where $A_1 = k/6\pi rD_0$, $A_2 = \exp(-S_m/R)$, $B = H_m$, $C = \exp(-S_d/R)$, $D = H_d$, and $D_0 = fg\lambda^2 z p_0 v_0$.

Here H_d and S_d are the enthalpy and entropy of configuron (broken bond) formation, H_m and S_m are the enthalpy and entropy of configuron motion, f is the correlation factor, g is a geometrical factor ($\sim$1/6), λ is the average jump length, z is the number of nearest neighbours and p_0 is a configuration factor, v_0 is the configuron vibrational frequency or the frequency with which the configuron attempts to surmount the energy barrier to jump into a neighbouring site. In contrast to many other approximations this equation can be used over wider temperature ranges and gives the correct Arrhenian-type asymptotes at high and low temperatures namely $\eta(T) \cong AT\exp(B/RT)$ and $\eta(T) \cong ACT\exp[(B+D)/RT]$ respectively. This correctly gives Arrhenian-type asymptotes at high and low temperatures with high activation energy of flow at low temperatures $Q_H = B + D$ and low activation energy at high temperatures $Q_L = B$.

Broken bonds weaken the bond lattice of a material and because of that the fluidity of amorphous materials is higher at higher temperatures. Bond breaking under the electron beam occurs due to both irradiation and thermal fluctuations, the higher the temperature and the electron flux density (intensity of irradiation) the higher the rate of production of broken bonds contributing to flow. If significant structural changes occur thermodynamic parameters of configurons under the electron beam (H_{di}, H_{mi}, S_{di} and S_{mi}) can be different from that for a non-irradiated material (H_d, H_{m}, S_d and S_m). These changes are particularly characteristic at high electron flux densities. However in a first approximation we can suppose that the irradiated material has approximately the same structure except formation of additional broken bonds. In this case we can assume that $H_{\mathrm{di}} \approx \mathrm{H}_d$, H_{mi}, $\approx \mathrm{H}_m$, $S_{\mathrm{di}} \approx S_d$ and $S_{\mathrm{mi}} \approx S_m$. Within such approximations using the same approach as in [38–40] we can readily find that the viscosity of irradiated amorphous materials is given by:

$$\eta_R(T) = \eta(T)/[1 + \alpha_e I_e[1 + C\exp(D/RT)]] \tag{11}$$

where $\eta(T)$ is the viscosity of an non-irradiated material and $\alpha_e I_e$ plays the role of dimensionless electron flux density. Note that at very low levels of radiation when $I_e \to 0$ the viscosity Eq. (11) reduces to known formula (16) for non-irradiated amorphous materials [38–40]. In contrast at very high levels of irradiation it shows that the viscosity decreases directly proportionally to the intensity of irradiation (I_e), e.g. gives the same results as Eq. (9).

Eq. (11) shows that the higher the electron flux density the higher the increase of fluidity. Moreover we can note that intensive electron beam irradiation changes the activation energy of viscous flow from characteristic high values $Q_H = B + D$ at low temperatures to low values $Q_L = B$, which in absence of radiation are characteristic only for high temperatures. As the low activation energy of

viscosity is exactly equal to the enthalpy of motion of bonds we conclude that the radiation-enhanced flow is indeed governed by bond motion rather than bond breaking which agrees with experimental data [11]. The smaller the temperature the more significant is the radiation-induced decrease of viscosity at the same electron flux density. Such type effects are similar to the effect of radiation-induced unbinding of alkalis in silicate glasses [45]. Note that in order to observe the radiation-induced fluidity either the electron flux densities should be enough high or the temperatures should be enough low.

To numerically estimate the viscosity of amorphous oxide materials under the electron beam we need data on thermodynamic parameters of bonds. These can be taken as from the non-irradiated materials in the first approximation. However the configuron parameters for glasses studied in this research are unknown from literature. Because of that we will illustrate the effect of electron beam irradiation in Fig. 9 for the soda lime silicate system where the thermodynamic data are available [39], for which $T_g = 777$ K, $f_c = 7.42 \times 10^{-4}$, $H_d = 331$ kJ/mol, $S_d = 44.03R$, $H_m = 293$ kJ/mol, $S_m = 24.40R$.

Three important points should be drawn from both Eq. (11) and Fig. 9:

(i) The decrease of viscosity by increase of electron flux density, I_e.
(ii) The presence of a threshold temperature, T_{th}, which is dependent on electron flux density with higher values at higher I_e. The appearance of T_{th} below which the effects of irradiation are significant is similar to that found in radiation-induced alkali ion exchange reactions [5,27,41] as well as to that found in electrical conductivity of irradiated glasses [42,43].
(iii) The step-wise decrease of activation energy of viscosity from the high values Q_H (which is characteristic for temperatures below the glass transition temperature) to low values Q_L (which are typical at temperatures high above the glass transition temperature).

Fig. 9 shows that even at relative low electron flux densities when radiation creates a relative small fraction of broken bonds, so that

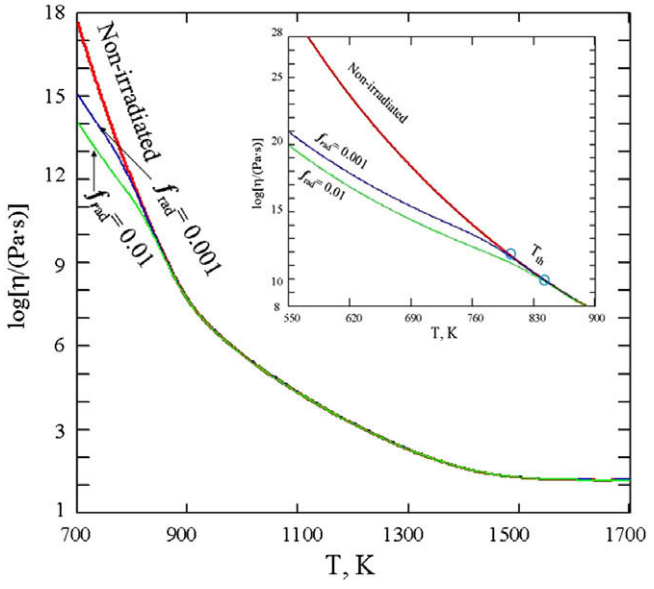

Fig. 9. Viscosities of non-irradiated and electron beam irradiated amorphous soda lime silicate system $70SiO_221CaO9Na_2O$ as a function of temperature for two dimensionless electron flux densities ($f_{rad} = \alpha_e I_e$) 0.01 and 0.001.

$f_{rad} = 0.001$, the viscosity of glass decreases by many orders-of-magnitude. The electron beam induced increase of fluidity is most evident at lower temperatures and is almost not detectable at high temperatures when the fluidity is high due to thermal effects. The lower the electron flux density f_{rad} the lower the temperature below which the radiation-induced fluidity can be observed. The activation energy of viscous flow in irradiated soda lime silica glass has changed at relative low temperatures ($T < 800$ K) from characteristic high values Q_H (634 kJ/mol) to low values Q_L (293 kJ/mol) which are observed only at high temperatures for non-irradiated glasses [38–40,41].

5. Discussion

Due to surface tension forces fluidisation of glasses at enough high electron flux densities can result in modification of nano-sized particles and holes, e.g. nano-patterning effects such as those observed here as well as reported in [26]. The consequences of electron beam induced increase of fluidity could be different and will also dependent on sample size. The process of fluidity enhancement is first observed as minor roundening of the most rough corners of specimen surfaces. This first stage occurs at the same timescale than other, more frequently reported, irradiation phenomena in silicates, such as bubble formation, alkali accumulation [26,44] and nanoscale amorphous phase separation [22]. The full transformation of a non-spherical object (such as a fibre end) into a sphere is then a second stage which occurs after the other events have saturated. The example of Fig. 3 does not follow the pattern of the other events, and needs further exploration.

The mechanism by which the sample changes its form is that of viscous flow which is caused by the stress produced by surface tension forces. The tensile stress can be estimated using the Young–Laplace equation as $2\gamma/R$ where γ is the material–vapour interfacial energy and R is the sample end radius. The characteristic time of shape changes can be assessed as [45]:

$$\tau_\eta = \eta_R(T)d/3\gamma, \tag{12}$$

where $d = 2R$ is the characteristic size of system. The larger the characteristic size the longer the time required to observe changes caused by electron beam induced fluidisation. From the observations behind Figs. 1 and 2, an assessment of electron beam reduced viscosity of borosilicate glasses using (12) is possible, and accounting that the characteristic interfacial energy of silicate glasses is of the order of 0.4 J/m^2, an estimate for the characteristic viscosity of the order of 10^{11} Pa s is obtained. This shows that the glass is being transformed to a quasi-liquid state by the electron beam as its viscosity is lower than the viscosity attained at the glass–liquid transition. Fluidisation of glasses under the electron beam irradiation is caused by bond breaking by electrons and can occur at minimal thermal effects, practically without heating. The fluidisation occurs only in the irradiated volume and because of minimal thermal effects does not affect the surrounding areas. Because of that electron beam fluidisation can be used for accurate nano-patterning and can be potentially useful for dense (nano-scale) information writing as commonly used for chalcogenide phases [46].

Finally it needs to be mentioned that surface tension in a quasi-melted stage is not the only possible force active in shape transformation. Due to the electron beam charging of the glass fragments, electrostatic forces could also induce migration of atoms such that a state and shape of material with minimum total field energy is achieved.

These experimental findings are in good agreement with the suggested model of radiation-induced unbinding of alkalis from the non-bridging oxygen sites, which predicts a radiation-facilitated migration of alkalis with a lower cation-selective activation energy [41]. We should note that conventional melting of these glasses

would otherwise require temperatures above 1400 °C, temperatures which are unlikely reached in an electron microscope. This conclusion is evidenced by numerous experiments on crystalline phases not melted in the electron beam.

An alternative view point is to treat the rigidity and viscosity of a glass network by rigidity percolation theory [47,48]. This theory relies crucially on the average coordination number via covalent bridges in a glass network. Electron irradiation induced bridge breaking could push the initially rigid glass below a threshold where it behaves floppy, which otherwise could only be achieved by altering modifier concentration.

While the main emphasis of our work is on an effect of basic physics and chemistry of glasses, the impact on nuclear applications can be easily derived. We have to distinguish phenomena based on (i) damage as a collective effect involving a high fraction of material or damage followed by instant annealing, and (ii) damage which accumulates from individual events. The spontaneous shape transformations above a intensity threshold would belong to group (i), less relevant for other irradiation environments. However, gradual increase in diffusivity, or gradual conversion of glass coordination and network type would belong to group (ii) and therefore are expected to behave similarly in our high dose short time electron experiments in comparison to any very low dose, very long time situation, whether by electrons or gamma rays, such as applicable for active nuclear waste vitrification.

6. Conclusions

Fluidisation or quasi-melting of micro- and nano-samples during TEM irradiation of glassy materials is shown to be caused by effective bond breaking processes induced by the energetic electrons in the electron beam. Assuming that the viscous flow is mediated by broken bonds we derived an explicit equation of viscosity (11) which gives the correct viscosities of non-irradiated glasses and shows a significant increase of fluidity (reduction of viscosity) and decrease of activation energy of flow for electron beam irradiated glasses. We found that the viscosity of electron beam irradiated silicate glasses significantly decreases to values of the order of 10^{11} Pa s which shows that the glass is being transformed to a quasi-liquid state by the electron beam.

Acknowledgements

The authors are grateful to W.J. Weber for advise on thermal effects on irradiation, to K.R. Whittle, B.E. Burakov, N. Bibler, A. Abramenkovs, E. Valcke, A. Vaidotas and O. Batyukhnova for fruitful discussions, and to X. Xu and P. Bingham for experimental help.

References

[1] J.F. Denatale, D.G. Howitt, Nucl. Instrum. Methods Phys. Res. B1 (1984) 489–497.
[2] D. Ehrt, W. Vogel, Nucl. Instrum. Methods Phys. Res. B 65 (1992) 1–8.
[3] W.J. Weber, R.C. Ewing, C.A. Angell, G.W. Arnold, A.N. Cormack, J.M. Delaye, D.L. Griscom, L.W. Hobbs, A. Navrotsky, D.L. Price, A.M. Stoneham, M.C. Weinberg, J. Mater. Res. 12 (1997) 1946–1978.
[4] W.J. Weber, R.C. Ewing, C.R.A. Catlow, T. Diaz de la Rubia, L.W. Hobbs, C. Kinoshita, Hj. Matzke, A.T. Motta, M. Nastasi, E.K.H. Salje, E.R. Vance, S.J. Zinkle, J. Mater. Res. 13 (1998) 1434–1484.
[5] M.I. Ojovan, W.E. Lee, New Developments in Glassy Nuclear Wasteforms, Nova Science Publishers, New York, 2007. 131pp.
[6] K. Trachenko, J. Phys.: Condens. Mater. 16 (2004) R1491.
[7] W. Primak, R. Kampwirth, J. Appl. Phys. 39 (1968) 5651–5658.
[8] N.F. Borrelli, C. Smith, D.C. Allan, T.P. Seward, J. Opt. Soc. Am. B 14 (1997) 1606–1615.
[9] C.A. Volkert, J. Appl. Phys. 70 (1991) 3521–3527.
[10] E. Snoeks, T. Weber, A. Cacciato, A. Polman, J. Appl. Phys. 78 (1995) 4723–4732.
[11] C.A. Volkert, A. Polman, Mater. Res. Soc. Symp. Proc. 235 (1992) 3–14.
[12] T.M. Mayer, E. Chason, A.J. Howard, J. Appl. Phys. 76 (1994) 1633–1643.
[13] N.F. Mott, Philos. Mag. B56 (1987) 257–262.
[14] P.M. Ajayan, S. Iijima, J. Am. Ceram. Soc. 75 (4) (1992) 999–1001.
[15] S.G. Mayr, Y. Ashkenazy, K. Albe, R.S. Averback, Phys. Rev. Lett. 90 (2003) 055505.
[16] L.W. Hobbs, Ultramicroscopy 23 (1987) 339–344.
[17] D.B. Williams, C.B. Carter, Transmission Electron Microscopy, Plenum Press, New York, 1996.
[18] L. Reimer, H. Kohl, Transmission Electron Microscopy: Physics of Image Formation, Springer, Heidelberg, 2008.
[19] S. Bysakh, M. Shimojo, K. Mitsuishi, K. Furuya, J. Vac. Sci. Technol. B 22 (2004) 2620.
[20] X.W. Du, B. Wang, N.Q. Zhao, K. Furuya, Scripta Mater. 53 (2005) 899–903.
[21] B. Wang, Y.H. Yang, G.W. Yang, Nanotechnology 17 (2006) 5916–5921.
[22] N. Jiang, J. Silcox, J. Appl. Phys. 92 (2002) 2310–2316.
[23] N. Jiang, J. Qiu, A. Ellison, J. Silcox, Phys. Rev. 68B (2003) 064207.
[24] N. Jiang, J. Silcox, J. Non-Cryst. Solids 342 (2004) 12–17.
[25] G. Möbus, J. Tsai, X.J. Xu, P. Bingham, G. Yang, Microsc. Microanal. 14 (Suppl. 2) (2008) 434–435.
[26] B.S. Xu, S.I. Tanaka, Acta Mater. 46 (1998) 5249–5257.
[27] G. Yang, G. Möbus, R. Hand, Micron 37 (2006) 433–441.
[28] A.K. Varshneya, Fundamental of Inorganic Glasses, Society of Glass Technology, Sheffield, 2006 (Chapter 4).
[29] S.B. Fisher, Radiat. Effects Defects Solids 5 (1970) 239–243.
[30] A.E. Curzon, J. Phys. D. Appl. Phys. 22 (1989) 295–301.
[31] M. Liu, L.Y. Xu, X.Z. Lin, Scanning 16 (1994) 1–5.
[32] I. Jencic, M.W. Bench, I.M. Robertson, M.A. Kirk, J. Appl. Phys. 78 (2) (1995) 974–982.
[33] A. Meldrum, L.M. Wang, R.C. Ewing, Am. Mineral. 82 (1997) 858–869.
[34] Y. Zhang, J. Lian, C.M. Wang, W. Jiang, R.C. Ewing, W.J. Weber, Phys. Rev. B 72 (2005) 094112.
[35] I.T. Bae, Y. Zhang, W.J. Weber, M. Higuchi, L.A. Giannuzzi, Appl. Phys. Lett. 90 (2007) 021912.
[36] K. Sun, L.M. Wang, R.C. Ewing, Mater. Res. Soc. Symp. Proc. 807 (2004) A158.
[37] G. Yang, EELS and STEM Studies of Borosilicate Glass/Precipitate Nanocomposite Systems, Thesis Submitted for the degree of Doctor of Philosophy, The University of Sheffield, 2007.
[38] M.I. Ojovan, W.E. Lee, J. Appl. Phys. 95 (2004) 3803–3810.
[39] M.I. Ojovan, K.P. Travis, R.J. Hand, J. Phys.: Condens. Mater. 19 (2007) 415107 (12p).
[40] M.I. Ojovan, Adv. Condens. Mater. Phys. (2008) 817829 (23p).
[41] M.I. Ojovan, W.E. Lee, J. Nucl. Mater. 335 (2004) 425–432.
[42] N.A. Elalaily, R.M. Mahamed, J. Nucl. Mater. 303 (2002) 44–51.
[43] M.B. Volf, Mathematical Approach to Glass, Elsevier, Amsterdam, 1988.
[44] N. Jiang, G.G. Hembree, J.C.H. Spence, J. Qiu, F.J. Garcia de Abajo, J. Silcox, J. Appl. Phys. Lett. 83 (3) (2003) 551–553.
[45] G.C. Kuczynski, J. Appl. Phys. 20 (1949) 1160–1163.
[46] M. Wuttig, N. Yamada, Nat. Mater. 6 (2007) 824–832.
[47] Y. Cai, M.F. Thorpe, Phys. Rev. B 40 (1989) 10535–10542.
[48] I. Abramov, R. Keding, C. Rüssel, J. Non-Cryst. Solids 272 (2000) 147–153.